Organization principles of dynamic three-dimensional genome architecture associated with centromere clustering states

Satya Dev Polisetty[1], Shuvadip Dutta[2], Rakesh Netha Vadnala[3], Dimple Notani[3], Ranjith Padinhateeri[4,5,6], Kaustuv Sanyal*[1,7]

[1]Molecular Mycology Laboratory, Molecular Biology and Genetics Unit, Jawaharlal Nehru Centre for Advanced Scientific Research, Bengaluru, India.
[2]Department of Physics, Indian Institute of Technology Bombay, Mumbai, India.
[3]National Centre for Biological Sciences, TIFR, Bengaluru, India.
[4]Department of Biosciences and Bioengineering, Indian Institute of Technology Bombay, Mumbai, India.
[5]Sunita Sanghi Centre of Aging and Neurodegenerative Diseases, Indian Institute of Technology Bombay, Mumbai, India.
[6] Koita Centre for Digital Health, Indian Institute of Technology Bombay, Powai, Mumbai, 400076, India
[7]Department of Biological Sciences, Bose Institute, Kolkata, India.

*sanyal@jncasr.ac.in, sanyal@jcbose.ac.in

This PDF includes:
Main text
References
Figures 1-5

Abstract

Fungal centromeres are clustered near microtubule organizing centers to help adopt the Rabl chromosomal organization. The role of centromere clustering in driving large-scale changes in structural and functional chromatin assembly remains unclear. Here, using Hi-C and super-resolution microscopy, we show that cell cycle-dependent centromere declustering and clustering states in *Cryptococcus neoformans* drive global changes in the 3D genome architecture. Centromeres and telomeres are scattered around the nuclear periphery at interphase[G1], and this arrangement constrains the inter-arm interactions within a chromosome, providing a unique interphase[G1] chromosome organization. Moreover, centromeres and telomeres are organized as compartments, segregating them from active euchromatic regions. Polymer modeling reveals that the transition from the unclustered to clustered centromere state during the cell cycle involves changes from a globular to an elongated chromosome architecture. Strikingly, while clustered centromeres replicate early in most yeasts, *C. neoformans* centromeres replicate late in S-phase, hinting a possible link between centromere clustering dynamics and *CEN* DNA replication timing. Overall, our study uncovers several unique organizational principles governing the dynamic genome architecture in an evolutionarily diverged basidiomycete yeast.

Significance

Chromosomes occupy the nuclear space in many ways. Primary chromosomal arrangements are such that centromere regions of different chromosomes either form a cluster, as in yeasts, or are scattered around the nuclear periphery, more common in metazoans. Exceptionally, centromeres show cell cycle stage-specific clustering in the basidiomycete fungus *Cryptococcus neoformans.* We show that the spatial positioning and the refractory nature of centromeres and telomeres shape the arrangement and large-scale organization of chromosomes in *C. neoformans*. Metazoan-like late-replicating centromeres in *C. neoformans* possibly favor the unclustered/scattered centromere state in S-phase, not commonly found in fungi. Our results not only highlight the remarkable genome plasticity of *C. neoformans* but also raise the possibility that centromere replication timing determines genome organization principles.

Introduction

Chromosomes in a eukaryotic cell are three-dimensionally organized in two recurring configurations based on the spatial positioning of centromeres and telomeres[1], Rabl and non-Rabl/Type-II. In the Rabl configuration, centromeres and telomeres are spatially separated within the nucleus and arranged in separate clusters. The clustered centromeres and the telomere cluster are located at the nuclear periphery, but these two clusters are spatially positioned on opposite ends of the nucleus. In contrast, the non-Rabl/type-II configuration is marked by the territorial arrangement of chromosomes, where individual centromeres and telomeres are scattered across the nucleus, sometimes forming subclusters. Well-studied fungi in the phylum of Ascomycota show the Rabl arrangement of chromosomes[2], but most metazoan chromosomes tend to adopt the non-Rabl configuration[2]. Strikingly, *Schizosaccharomyces pombe* and *Magnaporthe oryzae* genomes adopt the Rabl arrangement[3,4] except transient declustering of centromeres is observed at metaphase. In the fruit fly *Drosophila melanogaster,* the centromere clustering is developmental stage-specific. While chromosomes in embryonic nuclei display the Rabl configuration[5] with clustered

centromeres, more differentiated fly cells, such as spermatocytes[6] have unclustered centromeres as chromosomes adopt the non-Rabl organization. Metazoans, including humans, exhibit differentiation-specific clustering of centromeres with the nucleolus, which is lost in terminally differentiated cells[7]. Intriguingly, centromeres show a strong propensity to cluster around the nucleolus in human cancer cells[7] although the role of centromere clustering in cancer cells needs to be explored.

Apart from shaping the chromosome-scale architecture, spatial positioning and clustering of centromeres impact the regulation of several structural aspects of the genome, including the telomere bouquet formation during meiosis in *S. pombe*[8]. While the importance of centromere clustering in shaping the genome architecture and function is significant, functional and architectural differences involved in clustered and unclustered centromere states are underappreciated. In this study, we report that in the basidiomycete budding yeast, *Cryptococcus neoformans*[9], the centromere clustering states differ according to the cell cycle stages - centromeres are unclustered during interphase and gradually cluster during mitosis[9]. This unique feature of dynamic changes in chromosomal organization makes *C. neoformans* an attractive model to track the natural transition of two major chromosome arrangements that exist across species. While the spatial positioning of centromeres orchestrates the overall three-dimensional genome organization[10], *C. neoformans* holds the key to link chromosome architectural changes associated with centromere clustering during the mitotic cell cycle.

Results

C. neoformans genome switches between non-Rabl and Rabl configurations

The cell cycle stage-dependent spatial clustering of centromeres/kinetochores has already been reported in *C. neoformans*[9,11]. We identified the homolog of Protector of Telomeres (Pot1), a single-strand telomere DNA-binding protein[12] (Supplementary Fig. 1) in *C. neoformans*. GFP-Pot1 was expressed in a strain where centromeres were marked with mCherry-tagged CENP-A. Telomeres in G1 cells were visible as multiple puncta located at the nuclear periphery, similar to centromeres (Fig. 1a), unlike any polarized distribution observed in *Saccharomyces cerevisiae* or *S. pombe*[13-15]. Instead, centromeres and telomeres in *C. neoformans* show no prominent spatial clustering resembling interphase cells of metazoans such as humans[16]. Centromeres in *C. neoformans* appear to cluster during G2 and anaphase as chromosomes adopt the Rabl-like arrangement (Fig. 1a and b), typically observed in yeast species. While there are 14 chromosomes in *C. neoformans,* the number of telomere puncta observed in G1 cells is significantly less than 28, indicating telomeres form subclusters (Fig. 1c). We could not detect Pot1 signals in most metaphase cells when centromeres migrated into the daughter bud. Notably, while centromeres do not form a single punctum, 14 individual centromere puncta in each G1 cell could not be detected, indicating centromeres form subclusters[9]. To further resolve the spatial positions of centromeres and telomeres, we imaged cells using 3D Structured Illumination Microscopy (SIM[2]) (Fig. 1d). This approach revealed that centromeres and telomeres are indeed scattered across the nucleus and occupy non-overlapping spatially proximal positions in interphase^{G1} cells.

Interphase^{G1} genome is characterized by strong inter-telomere interactions

To study the cell cycle-associated changes in the genome organization of the *H99* strain of *C. neoformans*, we performed Hi-C in synchronized interphase^{G1} and mitotic cells at metaphase and anaphase (Supplementary Fig. 2 a, b and c), and generated whole genome

contact maps (Fig. 1e). Hi-C was performed in two replicates at each of these stages. To assess the reproducibility of Hi-C data sets, we calculated pair-wise Pearson correlation coefficients of the datasets binned at 8 kb. The results indicate high concordance among the biological replicates (Supplementary Fig. 2d).

A striking feature of contact maps of a genome with the Rabl configuration of chromosomes is the presence of strong inter-centromere interactions[17-19]. Centromeres in *C. neoformans* are regional and span between 21 to 64 kb[20]. Inspection of Hi-C maps from synchronized interphase^{G1}, metaphase, and anaphase cells of *C. neoformans* (Fig. 1e and f) reveals that features of the interphase^{G1} contact map are distinct from those of ascomycete yeasts possessing the constitutive Rabl organization[2]. Contact maps confirm that interphase^{G1} cells lack usual strong centromere interactions between the chromosomes, suggesting the non-Rabl metazoan-like chromosome arrangement (Fig. 1e, red squares and 1f and Supplementary Fig. 3a) in a fungal cell. In fact, inter-telomere interactions across the chromosomes are strongly enriched (Fig. 1e, green squares and 1f and Supplementary Fig. 3a). Such telomere-telomere interactions significantly reduce at metaphase, possibly due to chromatin compaction. The telomere interactions associated with left and right arms of the chromosomes remained uniform across stages (Fig. 1f, Supplementary Fig. 3a). While microscopic observations demonstrate the existence of multiple telomere puncta, Hi-C data support enriched telomere contacts, confirming subclustering of telomeres during interphase^{G1}, and anaphase. Perhaps the subcluster composition of telomeres is heterogeneous at the single cell level, which explains prominent telomere-telomere interactions in contact maps since Hi-C contacts are population averages. The metaphase stage in *C. neoformans* is characterized by a modest increase in inter-centromeric interactions as compared to interphase^{G1}, consistent with microscopy results where centromeres appear to be loosely clustered and stretched along the spindle during metaphase[9]. Hi-C data reveal that anaphase cells of *C. neoformans* exhibit features similar to the Rabl configuration, characterized by the strongest *trans*-chromosomal interactions mediated by centromeres as well as telomeres (Fig. 1e and f, Supplementary Fig. 3a).

Nuclear positioning of centromeres and telomeres shapes global chromosome architecture

Having established that *C. neoformans* chromosomes could adopt both the non-Rabl and Rabl-like arrangements in a cell cycle stage-specific manner, we sought to explore changes in the chromosomal organization facilitating the transition. A comparison of percent *cis* versus *trans* contacts across cell cycle stages reveals that the majority of interactions in interphase^{G1} chromosome are *cis*, restricted within the same chromosome as less than 20% of the contacts across the chromosomes were between different chromosomes (*trans*) (Supplementary Fig. 3b). On the other hand, metaphase and anaphase chromosomes exhibit a modest increase in *trans* contacts as compared to interphase^{G1} (Supplementary Fig. 3b). To visualize the differences in chromatin contacts across stages, we plotted observed/expected maps (Fig. 2a). A comparison of contact maps across stages identifies that pericentromeric regions are refractory to interact with the rest of the chromosome (Fig. 2a, solid ovals), a feature conserved in budding and fission yeasts[18,19]. Notably, subtelomeric regions at interphase^{G1} also behaved similar to centromeres (Fig. 2a, dashed ovals). This indicates the refractory nature of both pericentromeric and subtelomeric regions constrain the inter-/intra-arm interactions, thus shaping the non-Rabl interphase^{G1} chromosome organization (Fig. 2a, below). Unlike interphase^{G1}, subtelomeric regions at anaphase engage in extensive

183 interactions with the arms of the same chromosome (Fig. 2a, dashed oval). Across the stages,
184 interactions among the arms of a chromosome increased as the distance from the
185 centromeres increased (Fig. 2a, black box). The arm-arm interactions originating from
186 centromeres are more enriched at metaphase and anaphase, implying the folding of arms at
187 centromeres (Fig. 2a, below). Such arm-arm interactions adjacent to centromeres are absent
188 in the interphase^{G1} genome. Centromere-centered aggregate maps across stages yield a
189 similar trend (Fig. 2b, black boxes). These differences further confirm that the folding of
190 metaphase and anaphase chromosomes resembles the properties of chromosomes arranged
191 in the Rabl form. These aggregate maps also indicate that the pericentromeric interactions
192 within the arms are stronger in interphase^{G1} as compared to anaphase (Fig. 2b, dashed ovals),
193 revealing these regions are highly compacted in interphase^{G1}. In metaphase, the overall
194 increase in interactions around centromeres may be due to compaction of chromatin in
195 general. To test if the stage-dependent compaction changes are restricted only to
196 pericentromeric regions, we analyzed aggregate profiles of telomeres belonging to the left
197 arm and noticed that interactions along the diagonal remains similar across the stages
198 (Supplementary Fig. 4). To confirm these observations, we plotted average compaction
199 profiles for individual chromosomes across stages (Fig. 2c and Supplementary Fig. 5). Note
200 that the compaction profiles highlight the extent of local compaction within a specific
201 chromosome and thus a comparison across different Hi-C experiments may not be
202 appropriate. We observed that the regions flanking centromeres are highly compacted as
203 compared to the rest of the chromosome in interphase^{G1} and metaphase. Surprisingly, the
204 extent of compaction of these regions at anaphase is on par with the chromosome compaction
205 levels. In all three stages, namely interphase^{G1}, metaphase, and anaphase, telomeres
206 remained highly compacted.

207 Next, we studied the differences in local chromatin packing across the cell cycle stages. Visual
208 inspection of Hi-C maps at 2 kb resolution indicated the presence of strong self-interacting
209 domains, similar to the domains reported in fission yeast[18], in interphase^{G1} (Fig. 2d), To
210 quantify changes in the domain organization, we determined domain boundaries by
211 estimating genome-wide insulation scores[21] from interphase^{G1} Hi-C data and generated
212 aggregate Hi-C maps of identified domains (Fig. 2e). The analysis revealed the presence 40-
213 70 kb long domain-like structures in interphase^{G1} chromosomes (Supplementary Fig. 6). The
214 presence of these domains was significantly reduced during metaphase, likely due to the
215 overall compaction of chromosomes. Such domains started to appear during anaphase,
216 hinting at the gradual reestablishment of domain-like structures, a phenomenon observed in
217 humans[22]. The striking resemblance of the disappearance of the domain-like structure across
218 kingdoms of life is noteworthy. Based on these observations, we suggest that local as well as
219 global chromatin architecture and the spatial positioning of centromeres and telomeres shape
220 the cell cycle stage-specific chromosome reorganization.

221 To understand the difference in the nature of chromatin folding across mitotic stages, we
222 plotted intra-arm contact probability (*P*) over the genomic distance, *s*. *P(s)* values change in
223 a cell cycle stage-specific manner[23]. A power-law scaling between s^{-1} and $s^{-1.5}$ indicates a
224 fractal globule, and above $s^{-1.5}$ indicates an equilibrium globule. The *P(s)* of interphase^{G1}
225 uncovered two regimes of power-law scaling. Regions ranging from 10 to 100 kb exhibited
226 ~$s^{-0.93}$ and those above 100 kb showed $s^{-1.72}$ (Fig. 2f, below and Supplementary Fig. 7a). The
227 observed power-law scaling during interphase^{G1} in *C. neoformans* indicates that at distances
228 <100 kb, chromatin is organized as a fractal globule, and at >100 kb, chromatin exhibits the

229 properties of an unconstrained polymer. The metaphase stage has a slower rate of decay at
230 distances <100 kb with a power law scaling of $s^{-0.62}$, indicating compaction of the
231 chromosomes, and >100 kb, the decay was rapid with ~$s^{-1.31}$ (Fig. 2f, below and
232 Supplementary Fig. 7a), which is similar to metazoan metaphase chromosomes[23]. Anaphase
233 chromatin, rather strikingly, showed a uniform steep decay in contact frequency with values
234 s^{-1} and $s^{-1.1}$ for short and long distances, respectively (Fig. 2f, below and Supplementary Fig.
235 7a). This suggests that both at short and long distances, chromatin is folded as a fractal
236 globule. The above-mentioned features were observed for the arms of individual
237 chromosomes as well (Supplementary Fig. 7b-d). A comparison of interphase^{G1} and
238 anaphase *P(s)* curves reveals that contacts between regions spanning 20-100 kb are
239 enriched in interphase^{G1}, and the interphase^{G1} domains are of sizes 40-70 kb. We speculate
240 that the loss of contacts at 20-100 kb distances (Fig. 2f) perhaps corresponds to the observed
241 loss of strong domain-like structures in anaphase (Fig. 2e). On the other hand, contacts
242 spanning ~ 150 kb are enriched in anaphase, providing an explanation for the observed
243 increase in long-range contacts that encompass subtelomeric regions evident from O/E
244 maps. To further confirm that anaphase chromosomes indeed exhibit enhanced distal/long-
245 range contacts, we plotted the Distal Contact Index (DCI). DCI quantifies the ratio between
246 distal and local contact strengths, providing a measure of the extent of long-range chromatin
247 interactions. DCI analysis revealed an enrichment of distal contacts >70 kb across all
248 chromosomes during anaphase as compared to interphase^{G1} (Supplementary Fig. 8a and b).
249 The differences in the domain organization in interphase^{G1} and anaphase stages, combined
250 with the changes in the decay pattern of *P(s)* curves, confirm that anaphase chromatin is less
251 compact than interphase^{G1} with reduced short-range interactions but more prominent long-
252 range interactions.

253 **Centromeres and telomeres form separate compartments in interphase^{G1}**

254 Since the pericentromeres and subtelomeres are refractory to interacting with the rest of the
255 genome, we generated a correlation matrix[24] to test if these regions behave similarly to the A
256 and B compartments observed in metazoans[24-28]. Though we did not observe a plaid pattern
257 that is present in metazoan contact maps[24], we noticed that both pericentromeric and
258 subtelomeric regions in *C. neoformans* remained in one compartment, referred to as the
259 centromere-telomere (CT) compartment, and the rest of the chromosome remained in the
260 non-CT compartment (Fig. 3a, left panel). This pattern was lost at anaphase, where only
261 pericentromeric regions are segregated from the rest of the genome (Fig. 3a, right panel).
262 Next, we performed eigendecomposition[24] and the first eigen vector was used to estimate the
263 positions of the compartments. The principal component (PC1) indicated the presence of two
264 large compartment-like structures in all chromosomes, except for chromosomes 2 and 12.
265 The CT compartments were enriched with H3K9me2 and H3K27me3 marks and have
266 reduced transcription (Fig. 3b and c, Supplementary Fig. 9). To find out if these CT
267 compartments physically interact among each other, we plotted interactions whose $\log_2$
268 observed/expected ratio is >3 using circos (Fig. 3b). Indeed, strong interactions were detected
269 between subtelomeric regions of different chromosomes within the CT compartment but not
270 with centromeres. These observations demonstrate that the *C. neoformans* interphase^{G1}
271 genome is explicitly organized into two large euchromatic and heterochromatic
272 compartments.

273

Modeling chromatin architectural states associated with clustered and unclustered centromeres

To better understand the overall 3D folding features of the chromosomes in Rabl and non-Rabl states, we developed a polymer model by coarse-graining the *Cryptococcus* genome into 14 flexible chains made of beads connected by springs, each representing one chromosome. Each bead represents a 10 kb chromatin segment, which is equivalent to about 50 nucleosomes. The polymer models were built in two sequential stages (Fig. 4a) to progressively reconstruct the global 3D genome organization. First, we generated an ensemble of individual chromosome conformations guided by Hi-C data. Next, chromosome-wise conformation states, the number of centromere and telomere clusters, and the nuclear volume were integrated to simulate the whole genome by placing all 14 chromosomes within a spherical confinement, mimicking the physical boundaries of the nucleus. Physical constraints due to stage-specific clustering of centromeres and telomeres (Fig. 4b) were introduced based on microscopy data (Fig. 1a). Visual inspection of the polymer models revealed that interphase[G1] chromosomes form compact globular structures, whereas anaphase chromosomes are axially elongated and less compact (Fig. 4c and d). Features of anaphase chromosomes are more Rabl-like (Fig. 4d). Intriguingly, during anaphase, regions surrounding centromeres of chromosomes appeared to be more elongated as compared to interphase[G1]. Perhaps, the axial elongation of pericentromeric regions facilitates clustering of centromeres of different chromosomes in a confined nuclear space. To quantify these changes, we estimated the radius of gyration (R_g) and asphericity (Fig. 4e) of polymer models of individual chromosomes at both stages. Interphase[G1] chromosomes exhibited lower R_g and asphericity values, indicating more globular properties at interphase[G1] than at anaphase. Thus, the polymer modeling helped us conclude that the shift from the non-Rabl configuration to the Rabl-type is associated with large-scale restructuring of chromosome organization.

Late-replicating centromere and telomere regions are positioned at the nuclear periphery

The spatial proximity of centromeres and telomeres and their compartmentalization from the rest of the genome during interphase[G1] prompted us to test whether the genome is organized according to DNA replication timing as well. Several studies suggest a link between the 3D genome architecture and DNA replication timing[29]. Various parts of a genome are replicated at different time intervals within the S-phase. To estimate replication timing, we used sort-seq[30,31] to measure the DNA copy number changes in replicating (S) cells relative to the non-replicating cells (G1). While in G1, the DNA copy number remains uniform, the copy number of different parts of the genome differs at S phase depending on the time of replication. Using this approach, we generated replication timing profiles of all 14 chromosomes of *C. neoformans* (Fig. 5a). A z-score >0 (methods) indicates early replicating and <0 indicates late replicating genomic segments. Centromeres and their flanks showed a dip in z-score values compared to other genomic regions. Similarly, subtelomeric regions (50 kb from the ends[32]) also exhibited a dip. These results helped us conclude that both centromeres and telomeres are late replicating, unlike the ascomycete fungi such as *S. cerevisiae*, *S. pombe,* and *Candida albicans*[33-35], where centromeres are one of the earliest replicating regions, and telomeres replicate late in S phase. These observations, although unexpected, establish that the replication timing of centromeres and telomeres in *C. neoformans* is similar to metazoans[36,37] rather than the yeast species analyzed to date. Next, we investigated if the early and late replicating regions fall within two different genomic compartments that were identified earlier.

320 Indeed, the late replicating regions are found to be associated with CT compartments (Fig.
321 5b), and the early replicating regions belong to non-CT compartments. These observations
322 provide experimental support that both physical and functional properties/states of chromatin
323 dictate the interphase[G1] genome organization. Next, we investigated if the observed late-
324 replicating regions and heterochromatin are positioned towards the periphery of the nucleus.
325 We mapped the replication timing (z-score) values and the ChIP enrichment values of
326 genome-wide heterochromatin marks on the polymer model. This analysis revealed that most
327 late-replicating and heterochromatic regions are positioned towards the periphery (Fig. 5c, d,
328 e and f and Supplementary Videos 1 and 2). This was unlike what was reported in budding
329 yeast, where a "replication wave" like structure[38] is proposed to be present in which
330 heterochromatic regions such as centromeres are enriched with early firing origins and
331 telomeres are enriched with late firing origins that are arranged in a polarised fashion.

332 **Discussion**

333 Here we report the 3D genome organization and DNA replication timing of the human
334 pathogenic fungus *C. neoformans*. Using Hi-C, microscopy, and polymer modeling
335 approaches, we provide evidence that the *C. neoformans* genome dynamically switches
336 between two major chromosome configurations, the non-Rabl and Rabl, during the cell cycle.
337 Our results demonstrate spatial positioning of centromeres and telomeres influences the
338 overall organization of the chromosomes. Microscopic observations confirm that interphase[G1]
339 chromosomes in *C. neoformans* adopt the non-Rabl arrangement as centromeres and
340 telomeres, occupy spatially proximal positions at the nuclear periphery (Fig. 5g). This is in
341 striking contrast to the Rabl configuration observed in most ascomycete yeasts[13-15,17,39-42]. We
342 show that centromeres dynamically cluster and decluster during the cell cycle, whereas
343 telomeres remain in subclusters all throughout. The Hi-C data strongly support the previously
344 reported microscopic observation[9] that the centromeres gradually cluster in *C. neoformans*
345 during the cell cycle progression. Interphase[G1] Hi-C data indicate that pericentromeric and
346 subtelomeric regions form separate CT compartments and avoid interactions with the rest of
347 the genome. As a result, an interphase[G1] chromosome is organized into three distinct blocks:
348 a) euchromatin, b) the telomere block, and c) the centromere block. Centromere and telomere
349 blocks constrain the overall organization of the interphase[G1] chromosome by acting as an
350 insulator. Though heterochromatin and euchromatin are well segregated in fungi[18,19], the
351 above mode of arrangement is unique in fungi studied so far. As expected, chromosomes
352 undergo a dramatic reorganization as interphase[G1] chromosomes transit from the non-Rabl to
353 the Rabl-like configuration. In anaphase, only pericentromeric compartments exist, and the
354 subtelomeric regions engage in long-range interactions with the arms of the chromosomes.
355 Perhaps the polarised arrangement of centromeres and telomeres in the Rabl configuration
356 masks the insulator effect of telomeres. The pericentromeric regions of anaphase are
357 decondensed as compared to the rest of the genome. This is intriguing as in *S. pombe,*
358 heterochromatin factors compact pericentromeric regions and promote inter-arm interactions
359 between pericentromeric regions[18]. It will be interesting to investigate if the loss of
360 pericentromere compaction promotes centromere clustering during anaphase in *C.*
361 *neoformans*. Though there are differences in global chromosome organization, locally,
362 chromatin in interphase[G1] is folded into strong self-interacting domain-like structures reported
363 in *S. cerevisiae*, *S. pombe,* and *V. dahliae*[18,41,43]. The local chromatin organization also
364 significantly differs between interphase[G1] and anaphase in *C. neoformans*. As expected, the
365 robust domain-like structures apparent in interphase[G1] disappear in metaphase owing to

366 compaction. On the other hand, these domain-like structures are reestablished during the
367 transition from anaphase to interphase[G1] of the next cell cycle.
368
369 A comparative study across several species of eukaryotes revealed that condensin II plays an
370 important role in shaping the genome architecture across different species[1]. The presence of
371 both condensin I and II promotes type-II/non-Rabl configuration, where chromosomes form
372 territories. Most fungi lack condensin II subunits and thus favor the Rabl configuration[1].
373 Though *C. neoformans* lacks condensin II subunits, it can organize its chromosomes in a non-
374 Rabl configuration. A recent study in *Arabidopsis thaliana*[44] reported that condensin II and the
375 linker of the nucleoskeleton and cytoskeleton (LINC) complex proteins help establish the non-
376 Rabl configuration in interphase cells after exiting from mitosis. It has been shown in *C.*
377 *neoformans*[9,45] that both microtubules and a LINC complex protein, Sad1, are required for
378 timely centromere clustering. Similarly, the cytoskeleton may regulate the clustering and
379 declustering of centromeres, and to accommodate these dynamic changes, chromatin alters
380 its folding properties independent of condensin II. Condensin II has been repeatedly gained
381 or lost across many eukaryotic lineages[46]. Perhaps the presence of condensin II locks the
382 genome in type II configuration, and its loss offers flexibility to change the genome
383 organization to suit the needs of an organism.
384
385 In this study, we also provide evidence that, like other organisms, telomeres and subtelomeric
386 regions are late replicating in *C. neoformans*. Whereas, unlike other yeasts studied,
387 centromeres are late replicating. Late replicating centromere and telomere regions occupy
388 spatially proximal positions (Fig. 5c) and are spatially sequestered as separate compartments
389 from the relatively early replicating euchromatic regions, in contrast to the Rabl configuration
390 of most budding yeasts. This raises the question of whether the relative position of
391 centromeres with respect to that of telomeres within the nucleus influences centromere
392 replication timing in general. For example, in *S. pombe*, chromosomes are arranged in the
393 Rabl configuration, and centromeres bind to Swi6/HP1 and recruit DDK[47], causing
394 centromeres and their proximal regions to replicate early despite being heterochromatic.
395 Meanwhile, at telomeres, the presence of PP1 phosphatase creates conditions that are
396 refractory for the initiation of replication[48]. As a result, both centromeres and telomeres are
397 present in different microenvironments that influence their replication timing[48,49]. Forced
398 tethering of DDK to sub-telomeres did not advance the replication timing of telomeres like that
399 of pericentromeric regions, suggesting that telomeric chromatin can hinder the recruitment of
400 replication factors and delay its early replication[47,50]. Similarly, in *C. albicans*, a replication
401 initiation protein Orc4 is enriched at the centromere cluster, and its concentration gradually
402 reduces towards the telomeres. This proposed Orc4 gradient may, in principle, create
403 conditions contributing to early and late firing of centromeres and telomeres associated
404 origins respectively[51]. We hypothesize that telomeres may create an environment that
405 promotes late replication of regions associated with them. In the Rabl configuration,
406 centromeres are spatially separated from telomeres, whereas in non-Rabl, as observed in *C.*
407 *neoformans,* the proximity of centromeres to telomeres may hinder early replication of
408 centromeres. To verify if such a correlation exists in other organisms as well, we analyzed
409 organisms in which the organization and replication timing of the genome have already been
410 studied. In ascomycete yeasts possessing the Rabl configuration of chromosomes,
411 centromeres replicate early, and telomeres replicate late. Intriguingly, in maize, with a Rabl-
412 like arrangement, the centromeres replicate in mid S-phase[52]. On the other hand,
413 chromosomes in humans, chicken DT40 cells, and *A. thaliana* adopt the non-Rabl

414 arrangement, and centromeres replicate during mid to late S in these organisms[27,37,53-56].
415 These observations raise an intriguing link between the spatial positioning of telomeres and
416 centromeres in the nucleus and replication timing of these heterochromatic domains across
417 kingdoms of life. Altogether, our study highlights the conformational plasticity of the *C.*
418 *neoformans* genome and maps the structural changes associated with the Rabl and non-Rabl
419 conformational switching during the cell cycle. Most importantly, the conformation-switching
420 behavior of *C. neoformans* chromosomes makes it a unique model system for studying the
421 factors responsible for shaping the genome architecture in organisms that lack condensin II
422 and sheds light on the evolutionary diversity of the 3D genome architecture.

423 **Acknowledgements**

424 We thank members of the Sanyal laboratory for their support, discussion, and suggestions on
425 the work. We thank R. Siddharthan, The Institute of Mathematical Sciences, Chennai, and L.
426 Narlikar, IISER Pune, for the discussion and suggestions on the work. We thank V. Yadav,
427 Duke University, for the discussion and comments on the manuscript. We thank K. Hardwick
428 (University of Edinburgh) for the *MPS1* overexpression strain. We thank N. Nala and the in-
429 house flow cytometry facility at JNCASR. We thank the NGS facility at NCBS and A. Pandit
430 for sequencing Hi-C samples and for discussions on the DNA library preparation. This work
431 was supported by the Anusandhan National Research Foundation (ANRF), Department of
432 Science and Technology, Government of India (CRG/2023/001077) and intramural financial
433 support from JNCASR to K.S. K.S. is a JC Bose National Fellow (JCB/2020/000021). S.D.P.
434 acknowledges fellowship from ANRF (CRG/2023/001077), S.D. acknowledges fellowship
435 support from the PMRF, Ministry of Education, India. R.P. acknowledges support from Sunita
436 Sanghi Centre of Aging and Neurodegenerative Diseases (SCAN), IIT Bombay. The funders
437 had no role in study design, data collection and analysis, decision to publish, or preparation
438 of the manuscript.

439 **Competing interests**

440 The authors declare no competing interests.

441

442

443

444

445

446

447

448

449

450

451

452

453 **References**

454 1. Hoencamp, C. *et al.* 3D genomics across the tree of life reveals condensin II as a
455 determinant of architecture type. *Science* **372**, 984-989 (2021).
456 2. Torres, D.E., Reckard, A.T., Klocko, A.D. & Seidl, M.F. Nuclear genome organization in
457 fungi: from gene folding to Rabl chromosomes. *FEMS Microbiol Rev* **47**(2023).
458 3. Takahashi, K., Chen, E.S. & Yanagida, M. Requirement of Mis6 centromere connector
459 for localizing a CENP-A-like protein in fission yeast. *Science* **288**, 2215-9 (2000).
460 4. Yadav, V. *et al.* Cellular Dynamics and Genomic Identity of Centromeres in Cereal Blast
461 Fungus. *mBio* **10**(2019).
462 5. Marshall, W.F., Dernburg, A.F., Harmon, B., Agard, D.A. & Sedat, J.W. Specific
463 interactions of chromatin with the nuclear envelope: positional determination within
464 the nucleus in Drosophila melanogaster. *Mol Biol Cell* **7**, 825-42 (1996).
465 6. Bauer, C.R., Hartl, T.A. & Bosco, G. Condensin II promotes the formation of
466 chromosome territories by inducing axial compaction of polyploid interphase
467 chromosomes. *PLoS Genet* **8**, e1002873 (2012).
468 7. Rodrigues, A. *et al.* Nucleoli and the nucleoli-centromere association are dynamic
469 during normal development and in cancer. *Mol Biol Cell* **34**, br5 (2023).
470 8. Jimenez-Martin, A. *et al.* Centromere positioning orchestrates telomere bouquet
471 formation and the initiation of meiotic differentiation. *Nat Commun* **16**, 837 (2025).
472 9. Kozubowski, L. *et al.* Ordered kinetochore assembly in the human-pathogenic
473 basidiomycetous yeast Cryptococcus neoformans. *mBio* **4**, e00614-13 (2013).
474 10. Muller, H., Gil, J., Jr. & Drinnenberg, I.A. The impact of centromeres on spatial genome
475 architecture. *Trends Genet* **35**, 565-578 (2019).
476 11. Sridhar, S., Hori, T., Nakagawa, R., Fukagawa, T. & Sanyal, K. Bridgin connects the
477 outer kinetochore to centromeric chromatin. *Nat Commun* **12**, 146 (2021).
478 12. Baumann, P. & Cech, T.R. Pot1, the putative telomere end-binding protein in fission
479 yeast and humans. *Science* **292**, 1171-5 (2001).
480 13. Jin, Q.W., Fuchs, J. & Loidl, J. Centromere clustering is a major determinant of yeast
481 interphase nuclear organization. *J Cell Sci* **113 (Pt 11)**, 1903-12 (2000).
482 14. Guacci, V., Hogan, E. & Koshland, D. Centromere position in budding yeast: evidence
483 for anaphase A. *Mol Biol Cell* **8**, 957-72 (1997).
484 15. Funabiki, H., Hagan, I., Uzawa, S. & Yanagida, M. Cell cycle-dependent specific
485 positioning and clustering of centromeres and telomeres in fission yeast. *J Cell Biol*
486 **121**, 961-76 (1993).
487 16. Solovei, I. *et al.* Differences in centromere positioning of cycling and postmitotic
488 human cell types. *Chromosoma* **112**, 410-23 (2004).
489 17. Galazka, J.M. *et al.* Neurospora chromosomes are organized by blocks of importin
490 alpha-dependent heterochromatin that are largely independent of H3K9me3.
491 *Genome Res* **26**, 1069-80 (2016).
492 18. Mizuguchi, T. *et al.* Cohesin-dependent globules and heterochromatin shape 3D
493 genome architecture in S. pombe. *Nature* **516**, 432-435 (2014).
494 19. Duan, Z. *et al.* A three-dimensional model of the yeast genome. *Nature* **465**, 363-7
495 (2010).
496 20. Yadav, V. *et al.* RNAi is a critical determinant of centromere evolution in closely
497 related fungi. *Proc Natl Acad Sci U S A* **115**, 3108-3113 (2018).

498 21. Crane, E. *et al.* Condensin-driven remodelling of X chromosome topology during
499 dosage compensation. *Nature* **523**, 240-4 (2015).
500 22. Abramo, K. *et al.* A chromosome folding intermediate at the condensin-to-cohesin
501 transition during telophase. *Nat Cell Biol* **21**, 1393-1402 (2019).
502 23. Naumova, N. *et al.* Organization of the mitotic chromosome. *Science* **342**, 948-53
503 (2013).
504 24. Lieberman-Aiden, E. *et al.* Comprehensive mapping of long-range interactions reveals
505 folding principles of the human genome. *Science* **326**, 289-93 (2009).
506 25. Rowley, M.J. *et al.* Evolutionarily conserved principles predict 3D chromatin
507 organization. *Mol Cell* **67**, 837-852 e7 (2017).
508 26. Dong, P. *et al.* 3D chromatin architecture of large plant genomes determined by local
509 A/B compartments. *Mol Plant* **10**, 1497-1509 (2017).
510 27. Rao, S.S. *et al.* A 3D map of the human genome at kilobase resolution reveals
511 principles of chromatin looping. *Cell* **159**, 1665-80 (2014).
512 28. Dixon, J.R. *et al.* Topological domains in mammalian genomes identified by analysis
513 of chromatin interactions. *Nature* **485**, 376-80 (2012).
514 29. Nathanailidou, P., Taraviras, S. & Lygerou, Z. Chromatin and nuclear architecture:
515 shaping DNA replication in 3D. *Trends Genet* **36**, 967-980 (2020).
516 30. Muller, C.A. & Nieduszynski, C.A. Conservation of replication timing reveals global and
517 local regulation of replication origin activity. *Genome Res* **22**, 1953-62 (2012).
518 31. Koren, A., Soifer, I. & Barkai, N. MRC1-dependent scaling of the budding yeast DNA
519 replication timing program. *Genome Res* **20**, 781-90 (2010).
520 32. Dumesic, P.A. *et al.* Product binding enforces the genomic specificity of a yeast
521 polycomb repressive complex. *Cell* **160**, 204-18 (2015).
522 33. Raghuraman, M.K. *et al.* Replication dynamics of the yeast genome. *Science* **294**, 115-
523 21 (2001).
524 34. Kim, S.M., Dubey, D.D. & Huberman, J.A. Early-replicating heterochromatin. *Genes*
525 *Dev* **17**, 330-5 (2003).
526 35. Koren, A. *et al.* Epigenetically-inherited centromere and neocentromere DNA
527 replicates earliest in S-phase. *PLoS Genet* **6**, e1001068 (2010).
528 36. Massey, D.J. & Koren, A. Telomere-to-telomere human DNA replication timing
529 profiles. *Sci Rep* **12**, 9560 (2022).
530 37. Ten Hagen, K.G., Gilbert, D.M., Willard, H.F. & Cohen, S.N. Replication timing of DNA
531 sequences associated with human centromeres and telomeres. *Mol Cell Biol* **10**, 6348-
532 55 (1990).
533 38. Lazar-Stefanita, L. *et al.* Cohesins and condensins orchestrate the 4D dynamics of
534 yeast chromosomes during the cell cycle. *EMBO J* **36**, 2684-2697 (2017).
535 39. Thakur, J. & Sanyal, K. A coordinated interdependent protein circuitry stabilizes the
536 kinetochore ensemble to protect CENP-A in the human pathogenic yeast Candida
537 albicans. *PLoS Genet* **8**, e1002661 (2012).
538 40. Guin, K. *et al.* Spatial inter-centromeric interactions facilitated the emergence of
539 evolutionary new centromeres. *Elife* **9**(2020).
540 41. Torres, D.E. *et al.* Implications of the three-dimensional chromatin organization for
541 genome evolution in a fungal plant pathogen. *Nat Commun* **15**, 1701 (2024).
542 42. Winter, D.J. *et al.* Repeat elements organise 3D genome structure and mediate
543 transcription in the filamentous fungus Epichloe festucae. *PLoS Genet* **14**, e1007467
544 (2018).

545 43. Hsieh, T.H. *et al.* Mapping nucleosome resolution chromosome folding in yeast by
546 Micro-C. *Cell* **162**, 108-19 (2015).
547 44. Sakamoto, T. *et al.* Two-step regulation of centromere distribution by condensin II
548 and the nuclear envelope proteins. *Nat Plants* **8**, 940-953 (2022).
549 45. Yadav, V. & Sanyal, K. Sad1 spatiotemporally regulates kinetochore clustering to
550 ensure high-Fidelity chromosome segregation in the human fungal pathogen
551 Cryptococcus neoformans. *mSphere* **3**(2018).
552 46. Hirano, T. Condensins: universal organizers of chromosomes with diverse functions.
553 *Genes Dev* **26**, 1659-78 (2012).
554 47. Hayashi, M.T., Takahashi, T.S., Nakagawa, T., Nakayama, J. & Masukata, H. The
555 heterochromatin protein Swi6/HP1 activates replication origins at the
556 pericentromeric region and silent mating-type locus. *Nat Cell Biol* **11**, 357-62 (2009).
557 48. Dave, A., Cooley, C., Garg, M. & Bianchi, A. Protein phosphatase 1 recruitment by Rif1
558 regulates DNA replication origin firing by counteracting DDK activity. *Cell Rep* **7**, 53-
559 61 (2014).
560 49. Tazumi, A. *et al.* Telomere-binding protein Taz1 controls global replication timing
561 through its localization near late replication origins in fission yeast. *Genes Dev* **26**,
562 2050-62 (2012).
563 50. Aparicio, O.M. Location, location, location: it's all in the timing for replication origins.
564 *Genes Dev* **27**, 117-28 (2013).
565 51. Sreekumar, L. *et al.* Orc4 spatiotemporally stabilizes centromeric chromatin. *Genome*
566 *Res* **31**, 607-621 (2021).
567 52. Wear, E.E. *et al.* Genomic analysis of the DNA replication timing program during
568 mitotic S phase in Maize (Zea mays) root tips. *Plant Cell* **29**, 2126-2149 (2017).
569 53. Feng, S. *et al.* Genome-wide Hi-C analyses in wild-type and mutants reveal high-
570 resolution chromatin interactions in Arabidopsis. *Mol Cell* **55**, 694-707 (2014).
571 54. Grob, S., Schmid, M.W. & Grossniklaus, U. Hi-C analysis in Arabidopsis identifies the
572 KNOT, a structure with similarities to the flamenco locus of Drosophila. *Mol Cell* **55**,
573 678-93 (2014).
574 55. Concia, L. *et al.* Genome-wide analysis of the Arabidopsis replication timing program.
575 *Plant Physiol* **176**, 2166-2185 (2018).
576 56. Shang, W.H. *et al.* Chromosome engineering allows the efficient isolation of
577 vertebrate neocentromeres. *Dev Cell* **24**, 635-48 (2013).

578

579

580

581

582

583

584

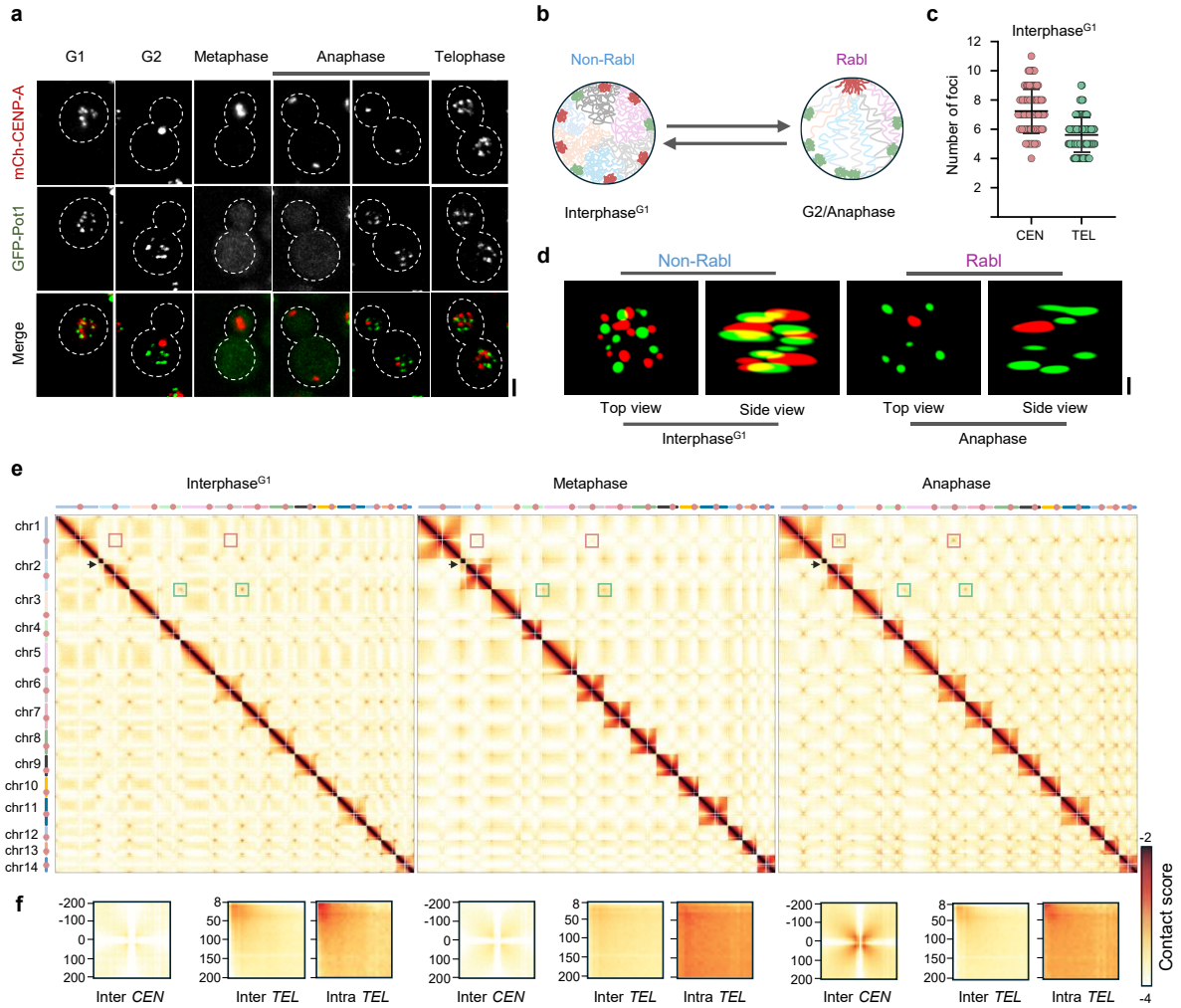

Fig. 1: The *C. neoformans* genome alternates between the non-Rabl and Rabl configurations during the cell cycle. a, Microscopic images of centromeres and telomeres marked by mCherry-CENP-A and GFP-Pot1, respectively, at different cell cycle stages. Scale bar, 2 µm. **b,** Schematic of the non-Rabl and Rabl arrangement of chromosomes. **c**, Quantification of the number of centromere or telomere puncta in interphase^{G1} stage, n=90 cells. The mean values are represented as a black bar. Error bars represent SD. **d**, 3D rendering of microscopic images of centromeres and telomeres of indicated cell cycle stages, Scale bar, 0.5 µm. **e**, Whole genome contact maps of interphase^{G1}, metaphase, and anaphase stages binned at 8 kb resolution. Chromosomes with centromeres marked in red circles are displayed on the left and at the top of the contact maps. Red and green squares on the maps represent inter-centromere and inter-telomere interactions, respectively. The black arrow marks the ribosomal DNA (rDNA) locus on chromosome 2. **f**, Aggregate Hi-C maps of inter-centromere/telomere and intra-telomere interactions (between left and right arms of the same chromosome), binned at 8 kb resolution, of all chromosomes. For calculating inter-/intra-telomere contacts, the left arm of the chromosomes was used. The color scale from yellow to brown represents low to high contact scores ($\log_{10}$), respectively. e and f panels share the same color scale.

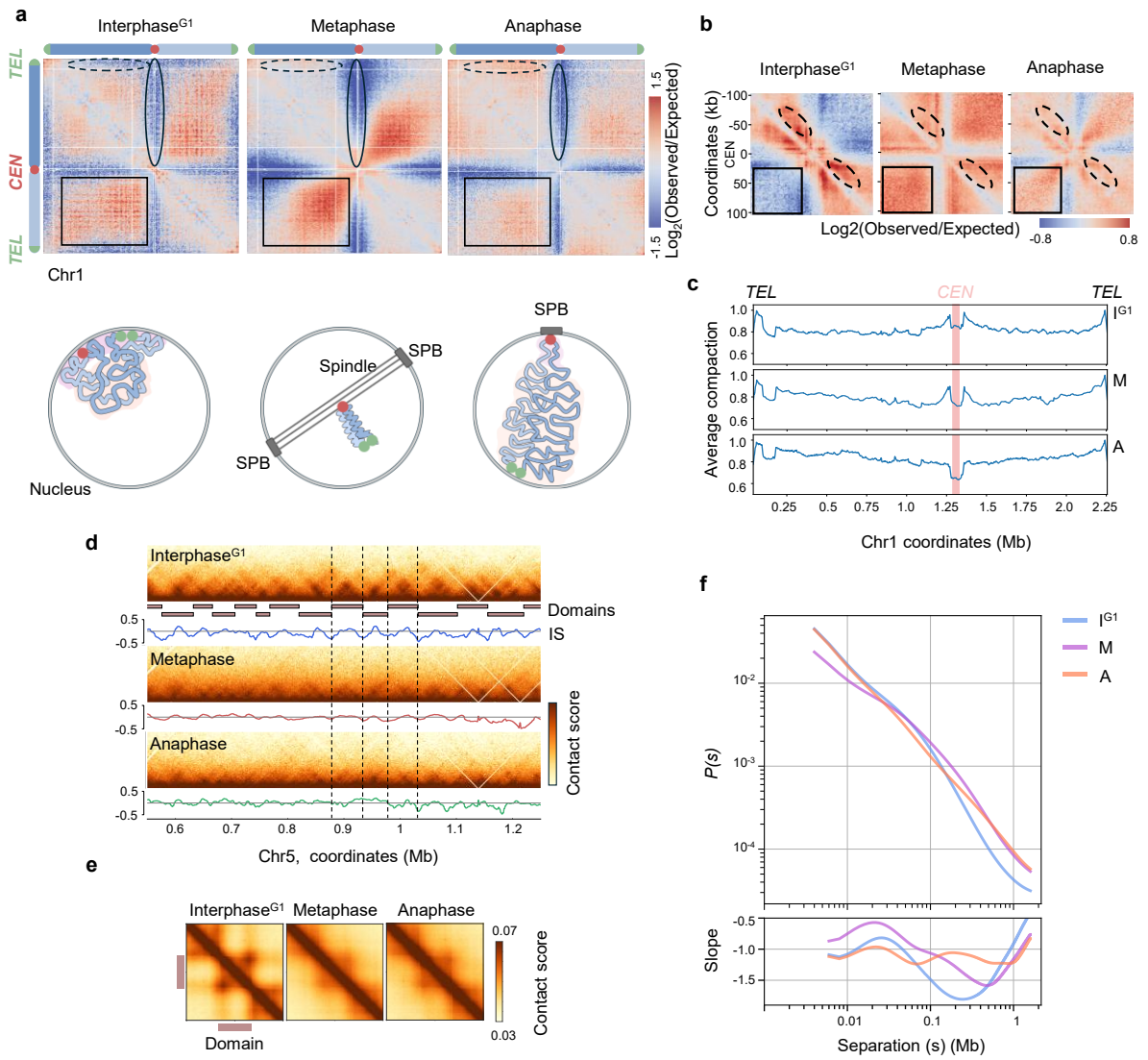

Fig. 2: Transition from the non-Rabl to Rabl configuration involves global chromatin decompaction. a, *Top,* Comparison of observed/expected maps of chromosome 1 of interphase^{G1}, metaphase, and anaphase stages, binned at 8 kb resolution. The blue to red color scale represents depletion and enrichment of contacts, respectively ($\log_2$ scale). Solid and dashed ovals on the maps denote the pericentromeric and subtelomeric regions, respectively. Black boxes highlight inter-arm interactions within a chromosome. *Below*, schematic highlighting structural changes in the chromosome organization across interphase^{G1}, metaphase, and anaphase stages. **b**, Observed/expected aggregate Hi-C maps of *cis*-contacts around 100 kb regions, surrounding all 14 centromeres, binned at 2 kb. Color scale as indicated above. Dashed ovals represent contacts within the arms of the chromosomes around centromeres. Black boxes represent inter-arm interactions around centromeres. **c**, Compaction profiles of chromosome 1 for the indicated stages. The x-axis represents chromosome coordinates, and the y-axis represents average compaction. The red-shaded rectangle highlights the centromere position. **d**, A region of chromosome 5 Hi-C contact map (binned at 2 kb) of interphase^{G1}, metaphase, and anaphase stages. Solid bars below interphase^{G1} contact map represent domains identified using interphase^{G1} Hi-C data. Insulation scores (IS) are indicated below each contact map. Dotted lines represent domain boundaries. The color scale from yellow to brown represents low to high contact scores, respectively ($\log_{10}$). **e**, Aggregate maps of domains across the three cell cycle stages (binned at 2 kb). The coordinates of the domain boundaries predicted using interphase^{G1} Hi-C data

were used to generate the aggregate maps of metaphase and anaphase. **f**, *Top,* contact frequency *P(s)* curves plot of Hi-C data obtained from interphase[G1], metaphase, and anaphase binned at 2 kb. *Below,* derivatives (d log P(s)/d log(s)) of the *P(s)* curves.

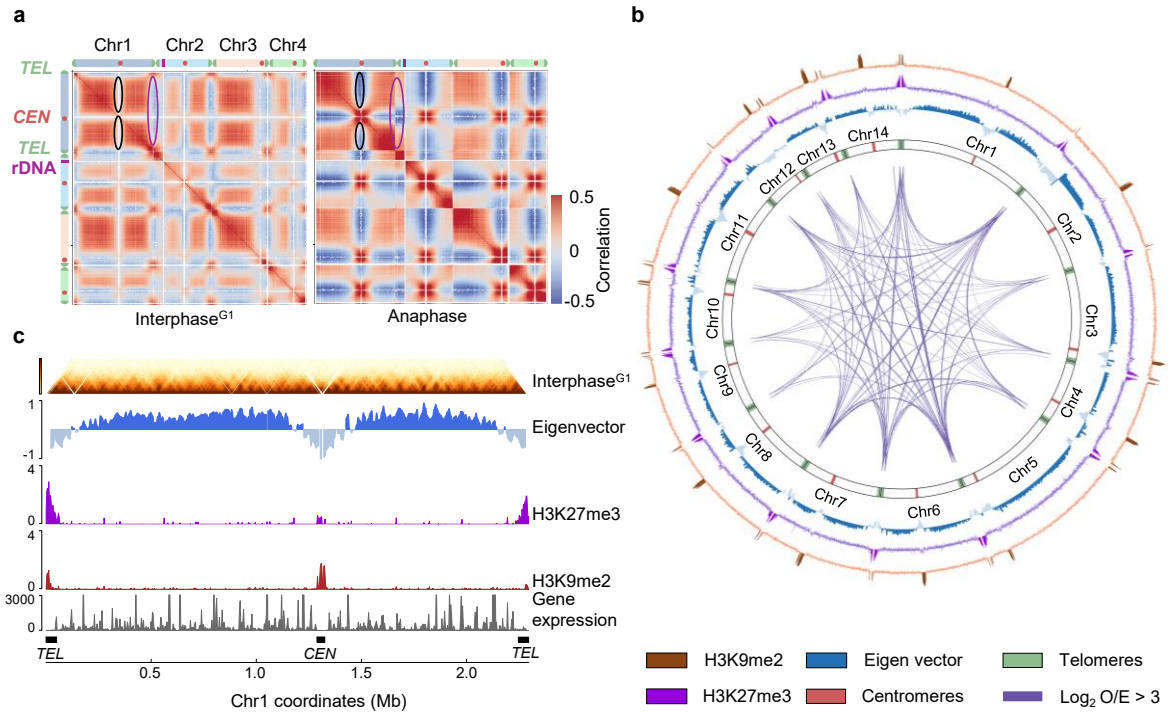

Fig. 3: Two-compartment-like organization of the *C. neoformans* interphase^{G1} genome. **a,** Correlation matrix of contacts for chromosomes 1 – 4 in interphase^{G1} and anaphase stages, binned at 8 kb. The color map from blue to red represents negative to positive correlation values. Black and violet ovals represent pericentromeric and subtelomeric compartments. **b**, Circular (circos) plot representing the interactions across the subtelomeric regions and the associated chromatin modifications and eigenvector. Violet links represent the strongest inter-chromosomal contacts whose log_2 (observed/expected) values are greater than 3. From outside to inside: H3K9me2 (brown), H3K27me3 (violet), eigenvector (blue), chromosomes marked with centromere (red) and telomeres (green) positions. **c**, Hi-C contact map of chromosome 1 binned at 2 kb at interphase^{G1}, corresponding tracks representing eigenvector, log_2 ChIP enrichment profiles of H3K27me3, H3K9me2, and gene expression levels are indicated below. Black bars represent centromeres and telomeres of chromosome 1. The color scale from yellow to brown represents low to high contact scores, respectively (log_{10}).

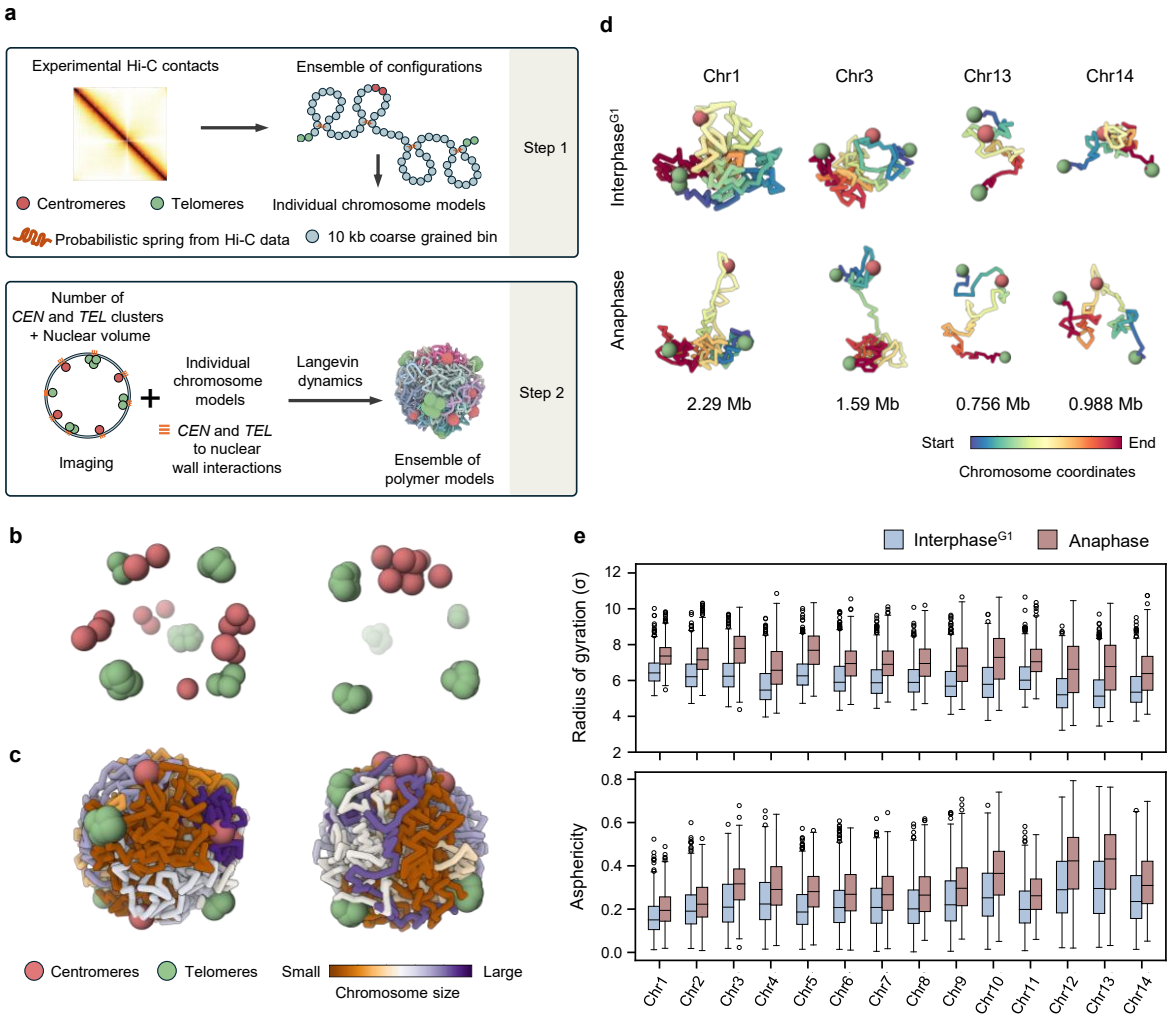

Fig. 4: Polymer modeling of the *C. neoformans* genome. a, Schematic of the steps followed for generating a polymer model of the *C. neoformans* genome. **b**, Representative snapshot of simulations of interphase^{G1} and anaphase, highlighting only the spatial distributions of centromeres and telomeres. **c**, Snapshot of interphase^{G1} and anaphase whole genome polymer models. The individual chromosomes are colored according to increasing chromosome sizes. **d**, Snapshots of the polymer models of large (chr1; metacentric and chr3; acrocentric) and small (chr13; acrocentric and chr14; metacentric) chromosomes from interphase^{G1} and anaphase stages, colored from one end to the other (start to end coordinates). **e**, *Top,* Box plots of radius of gyration (R_g) values of chromosomes at interphase^{G1} and anaphase. The higher the value, the more elongated the structure. *Below,* box plots of asphericity values estimated from the polymer models of chromosomes at the indicated stages. The lesser the value, the more globular the structures. The horizontal line inside the box represents the median, and the box denotes the interquartile range, 25% to 75%.

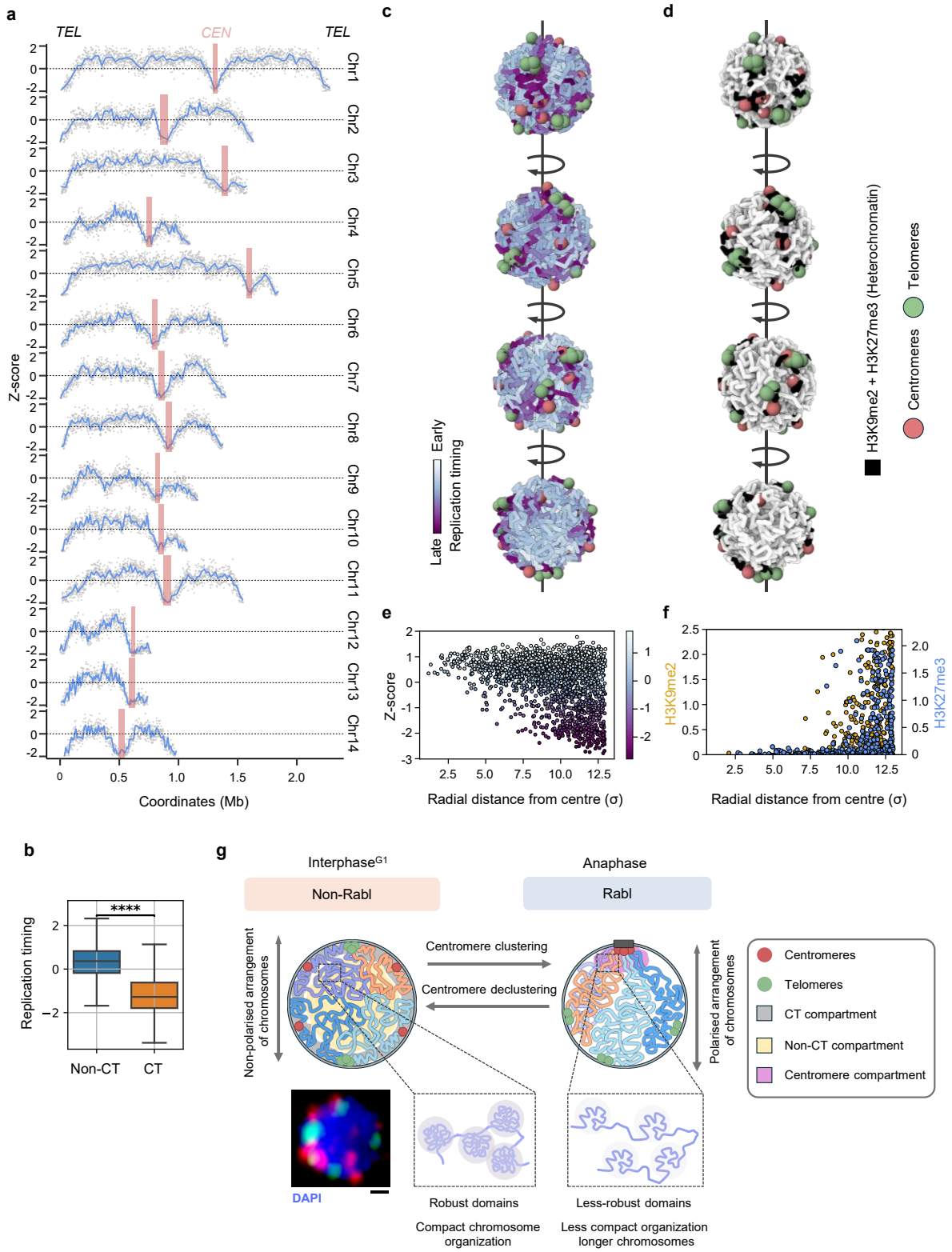

Fig. 5: Late replicating heterochromatic regions are located at the nuclear periphery, insulated from the rest of the genome. a, DNA replication profile of all fourteen chromosomes. Red shaded boxes indicate centromeric regions. The x-axis represents chromosome coordinates in Mb, and the y-axis represents the z-score. Values >0 indicate early replication, and values <0 indicate late replication. Gray dots represent 1 kb bins. The blue line represents LOESS-smoothed z-score values. **b**, Box plot of z-score values

715 (replication timing) of the indicated compartments. The Wilcoxon rank-sum test was used to
716 check the significance. **c-d**, Representative snapshot of the polymer simulation of
717 interphase[G1] genome overlaid with, (**c**) the replication timing (z-score) values and, (**d**) the
718 heterochromatin marks H3K9me2 and H3K27me3. Different views of the same structure are
719 shown. The green and red spheres represent centromeres and telomeres, respectively. The
720 blue-purple color gradient represents early to late replication timing. **e-f**, Scatter plot depicting
721 the radial distance of the 10 kb beads of the polymer model from the center of the nucleus to
722 the periphery with (**e**) replication timing and (**f**) ChIP enrichment profiles (log_2 values) of
723 H3K9me2 and H3K27me3 superimposed onto the beads. **g,** Model summarizing the changes
724 associated with the reorganization of the genome during the shift between Rabl and non-Rabl
725 states. In the model, a microscopy image of interphase[G1] nucleus stained with DNA-binding
726 dye DAPI and centromere and telomeres labelled with CENPA-mCherry and GFP-Pot1.
727 Scale bar, 1 μm.

728

729